

**T5 - Nanocrystalline and disordered materials**

T5 - P101

**STRUCTURE AND MECHANICAL PROPERTIES OF NANOCRYSTALLIZED Zr-BASED BULK METALLIC GLASSES****D. Fátay<sup>1</sup>, J. Gubicza<sup>2</sup> and J. Lendvai<sup>1</sup>**<sup>1</sup>*Department of General Physics, Eotvos Lorand University, Budapest, Hungary*<sup>2</sup>*Department of Solid State Physics, Eotvos Lorand University, Budapest, Hungary*

The bulk metallic glasses (BMGs) are in focus of materials science due to their unique mechanical properties. The high strength and low elastic moduli at room temperature and the high ductility above the glass transition temperature ( $T_g$ ) make BMGs very promising structural materials. The thermal stability of the amorphous structure is an important factor in the industrial application of these materials. In BMGs annealed above  $T_g$ , nanocrystalline particles may form. These precipitates have a great effect on the mechanical properties of the alloys, therefore it is important to find the relationship between the characteristic features of these particles (composition, size, shape, internal stresses etc.) and the mechanical behaviour.

In this work the effect of forming of nanocrystalline precipitates on the mechanical properties of Zr-based BMGs is studied. The phase composition and the microstructure of nanocrystallized specimens are investigated by X-ray diffraction. The crystallite size and the lattice strains are determined by X-ray line profile analysis. The mechanical behavior before and after crystallization is studied by indentation technique. The relationship between the mechanical properties and the structure of nanocrystallized BMGs are discussed.

*This work was supported by the Hungarian Scientific Research Fund, OTKA, Grant Nos. F-047057 and T-043247.*

T5 - P102

**ANNEALING BEHAVIOR OF Pd-Fe ALLOY NANOCLUSTERS PREPARED BY SEQUENTIAL ION IMPLANTATION IN SILICA****M. A. Tagliente<sup>1\*</sup>, C. de Julián Fernández<sup>2</sup>, G. Mattei<sup>2</sup>, M. Re<sup>2</sup>, M. Vittori Antisari<sup>3</sup> and P. Mazzoldi<sup>2</sup>**<sup>1</sup>*ENEA UTS MAT-COMP, Centro Ricerche Brindisi, SS.7 Appia km 714, 72100 Brindisi, Italy*<sup>2</sup>*Dip. Fisica, INFN Univ. Padova, via Marzolo 8, 54124 Padova, Italy*<sup>3</sup>*ENEA UTS MAT-COMP, Centro Ricerche Casaccia, via Anguillarese 301, 00060 S. Maria di Galeria Roma, Italy*

Composite materials formed by magnetic nanoparticles embedded in insulating matrices have attracted much attention due to their peculiar properties which are quite different from those of the corresponding bulk magnets, such as the superparamagnetism, the enhanced coercivity, the shift of the hysteresis loop, or the enhanced magnetic anisotropy. Moreover, in the nanoscopic regime, such properties are size-dependent. From a technological point of view, they are excellent candidates as magnetic recording media. Alloy-based nanoclusters offers the possibility to further tailoring the functional properties of the composite system to specific purposes by changing the alloy composition. Among the preparation procedures, sequential ion implantation has proved very effective to fabricate alloy-based nanoclusters in dielectric matrices. Moreover, the composite can be treated by a proper combination of treatments including irradiation by light ions or electrons, heat treatments in controlled atmosphere or pulsed laser irradiation, with several degrees of freedom in the preparation for effectively defining the structure of the clusters and so the composite performance.

Here, we present a study on the effects of heating treatments in reducing atmosphere performed at several temperatures on Pd-Fe alloys nanoclusters embedded in silica and prepared by sequential ion implantation. The evolution of the microstructural properties with the thermal treatments was investigated by Glancing Incidence X-Ray Diffraction combined with a pattern decomposition procedure for the quantitative analysis of the spectra. The experimental results were assessed by using Transmission Electron Microscopy. According to the results, the annealing in reducing atmosphere is found principally to promote the growth of the Pd-Fe nanoclusters while the alloys composition remain stable. These phenomena are accompanied by a strong Pd segregation.

\*corresponding author: M.A. Tagliente, e-mail address:

[antonella.tagliente@brindisi.enea.it](mailto:antonella.tagliente@brindisi.enea.it)



T5 - P103

**ELECTROCRYSTALLIZATION OF PT ON AU SUBSTRATES. XRD STUDY****I. Yu. Molina, L. M. Plyasova, S. V. Cherepanova, E. R. Savinova***Boriskov Institute of catalysis, pr. Lavrentieva 5, Novosibirsk, Russia*

To determine structural features responsible for adsorption characteristics and catalytic activity of highly dispersed electrodeposited catalysts, systematic X-ray diffraction study of the real structure of Pt electrodeposited on Au substrates was carried out. The influence of the deposition potential, electrochemical aging, model catalytic reactions and the texture of the Au support on the structural features of deposits have been analyzed. The samples were prepared via potentiostatic electrodeposition of Pt from  $\text{H}_2\text{PtCl}_6$  onto Au substrates. Deposition potential was varied in the range from 0.550 to 0.025 V. Amount of electrodeposited Pt was 0.5-1  $\text{mg}/\text{cm}^2$  and the estimated thickness varied from 0.20 to 0.80  $\mu\text{m}$ . The X-ray diffraction patterns were obtained using a URD-63 diffractometer (Germany) in  $\text{CuK}\alpha$  radiation with a scanning method within the angle interval  $2\theta = 30-90^\circ$  with  $0.02^\circ$  step and the exposition time of 10-20 s.  $\text{K}\alpha_2$  component of radiation was removed before processing the experimental data. To determine the instrumental broadening  $\gamma\text{-Al}_2\text{O}_3$  standard was used. The average lattice parameters were calculated with least-squares method using a program system "Polikristall" [1]. A single-line Voigt analysis method was used to calculate the crystallite size and strains in  $\langle 111 \rangle$  direction [2]. For some samples particle size distribution in the same direction have been calculated [3].

It has been shown that under the conditions employed highly defective electrolytic deposits are formed composed of nm-sized particles (10-30 nm). The structure of Pt nanoparticles is highly distorted which is expressed in rather high values of strains and decrease of lattice parameter. The crystallite size and lattice parameter decreases with an increase of the deposition potential while the strains increase. Calculations show that particle size distributions are bimodal with significant part of small size particles (less than 15 nm). There is good correspondence between

crystallite size obtained from Voigt analysis and particle size distribution.

It has been shown that electrochemical aging and model electrochemical reactions lead to the relaxation of the defect structure of electrodeposited Pt, which is expressed in an increase of lattice parameter and particle size. The abrupt decrease in the values of strains is observed for more defective samples obtained at low overvoltage (0.250 - 0.550 V).

It also has been shown that the texture of Au support (samples with  $\langle 200 \rangle$ ,  $\langle 311 \rangle$ ,  $\langle 220 \rangle$  Au texture were investigated) has no significant influence on the crystallographic orientation of Pt deposits. The differences in structural features for samples on textured supports are much weaker than that for deposits obtained on the identical supports but at different deposition potentials. The average particle size for Pt on the textured supports is 11-15 nm, all samples under investigation have practically equal values of lattice parameter and strains, and agree well with the early studied samples, obtained at the same deposition potential (0.300 V). Thus the data obtained shows that deposition potential is a key parameter determining structural characteristics of Pt electrodeposits.

*Acknowledgement*

*The study was supported by the Russian Foundation for Basic Research (projects N 01-03-33132, N 03-03-06348).*

- [1] S.V. Tsybulya, S.V. Cherepanova, L.P. Solovieva. J. *Struct. Chemistry* **37** (1996) 332 (in Russian).
- [2] J.I. Langford, R. Delhez, Th.H. Keijser and E.J. Mittemeijer. *Aust. J. Phys.* **41** (1988) 173.
- [3] Bertaut E. *Acta Crystallogr.* **3** (1959) 14.

T5 - P104

## PHASE TRANSITION IN NANOCRYSTALLINE ZnO

E.Grzanka<sup>1,2</sup>, S.Gierlotka<sup>1</sup>, S.Stelmakh<sup>1</sup>, B.Palosz<sup>1</sup>, T.Strachowski<sup>1</sup>, A.Swidarska-Sroda<sup>1</sup>, G.Kalisz<sup>1</sup>, W.Lojkowski<sup>1</sup>, F.Porsch<sup>3</sup>

<sup>1</sup>High Pressure Research Center, Sokolowska 29/37, 01142 Warsaw, Poland

<sup>2</sup>Institute of Experimental Physics, Hoza 69, 00681 Warsaw, Poland

<sup>3</sup>HASYLAB at DESY, Notkestr. 85, D-22603 Hamburg, Germany

Nanocrystals show novel physical and chemical properties different from those of the corresponding bulk material. In particular both temperature and pressure-induced phase transitions in polycrystalline materials show dependence on grain size. This work is dedicated to examination of the transition pressure of ZnO from wurtzite (B4) to rocksalt (B1) structure by in-situ synchrotron radiation X-Ray diffraction. Nanocrystalline zinc oxide powders with grain size 18, 22, 30 nm and coarse grain ZnO powder as a reference sample were examined with use of Diamond Anvil Cell up to 40 GPa.

Recently it has been reported that transition pressure, from wurtzite to rocksalt structure of 12 nm grain size ZnO is 15.1 GPa, i.e. by 5.6 GPa larger than similar transition in microcrystalline powder, 9.5 GPa [1,2]. We have examined similar behaviour for 18 nm and 30 nm ZnO, illustrated in Figs. 1 and 2. Fig.1 shows plot of the intensity ratio of the  $I_{200}$  (B1) to  $I_{100}$  (B4) peaks for 18 and 30 nm powder as a function of pressure where similar plots are showed for micro- and 12 nm ZnO [1]. The increase of the transition pressure with a decrease of the grain size conforms to the previous data [1]. Fig.2 shows changes of the intensity ratio of  $I_{100}$  to  $I_{002}$  Bragg reflections of B4 phase, which show very different shape for micro- and nanocrystalline powders. This suggest that there are different mechanisms of the transition from B4 to B1 phase in nano- and micron-size grains. We suggest that the strong increase of the ratio  $I_{100}$  to  $I_{002}$  for large grains results from a simultaneous growth of a number of domains of B1 phase in the low pressure in B4 phase what leads to very strong internal stresses. A single nano-grain tends to remain one phase structure and therefore the intensity ratio  $I_{100}$  to  $I_{002}$  of the primary phase B4 changes only very little. During increase of the external stress applied to the ZnO powders above the transition pressure there is larger increase of strain in 18 nm ZnO than in 30 nm powder, while in  $\mu\text{m}$  grain size sample no increase of micro-strain is observed up to 40 GPa pressure. We suggest that the increase of strains in nanograins is connected with a very large surface area of the grains (inter-grain interfaces) which obviously show different elastic properties than the bulk (interior of the grains) [3].

This work was supported by the Polish Committee for Scientific Research – grant PBZ/KBN-013/T08/30, the Polish –German Project POL-00/009, DESY-HASYLAB Project II-99-053 and in part by the EC Grant “Support for Centers of Excellence” No. ICA1-CT-2000-70005.

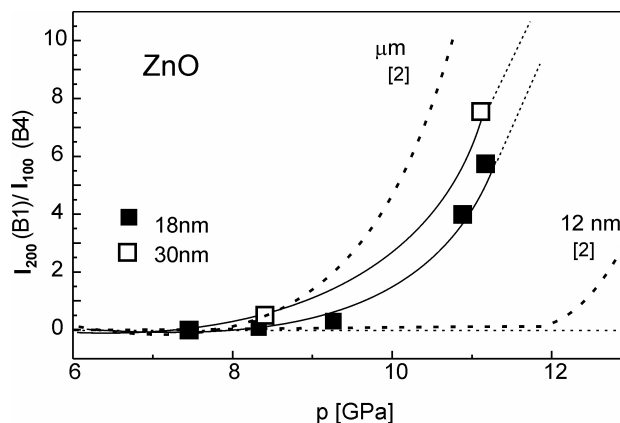


**Figure 1:** Changes of intensity ratio of 200 (B1) to 100 (B4) Bragg reflections with an increase of hydrostatic pressure for ZnO powder with 18 and 30 nm grains. Data for 12 nm and  $\mu\text{m}$  samples are from [2].

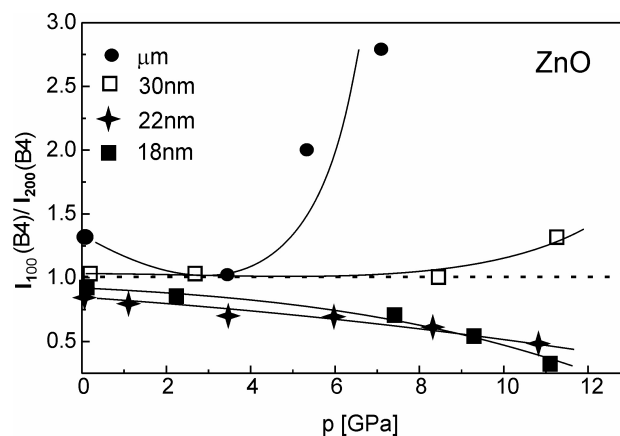


**Figure 2:** Changes of intensity ratio of 100 to 002 (B4) reflections below the transition pressure for micro- and nanocrystalline ZnO powders.

[1] F.Decremps, J.Zhang, C.Lieberman, *Europhys. Lett.* **51** (3), 268-274 (2000)

[2] F.J.Z.Jang, J.S.Olsen, L.Gerward, D.Frost, D.Rubie, J. Peyronneau, *Europhys. Lett.* **50** (1), 48-53 (2000)

[3] B.Palosz, Mechanics of Advanced Materials (Lecture Notes 4): Proceedings AMAS Course - MAM-2001, Ed.Z.Mróz, Center of Excellence for Advanced Materials and Structures, Warsaw 2002 pp. 235-306.



T5 - P105

## CHARACTERIZATION OF BULK MULTIWALL CARBON NANOTUBES

Jette Oddershede and Kenny Ståhl

Department of Chemistry, Technical University of Denmark, Building 207, DK-2800 Lyngby, Denmark.

Multiwall carbon nanotubes (MWCNTs) consist of rolled graphene sheets. As the tube properties are intimately linked to the bulk structure it is essential to be able to characterize this. The tubes are periodic in nature and therefore give rise to distinct diffraction peaks, thus diffraction is an excellent probe of bulk structure as opposed to TEM, which can only be used to determine local structure. The experimental diffractogram was recorded in transmission mode with a HUBER G670 Guinier camera ( $\lambda = 1.087\text{\AA}$ ) at beamline I711, MAXLAB (Lund, Sweden), on 50 mg of MWCNT sample pressed into a tablet.

Using the Debye formula the diffractograms for tubes with different structure can be simulated by summation over all the interatomic distances. The appearance of the

diffractograms depend on parameters such as the tube length and diameter, the repeat distance perpendicular to the tube, the number of concentric tubes, and the rolling direction (chiral or achiral tubes). Systematic variations of the parameters to determine the effects and correlations will be presented along with fits to experimental data. In the above example the peak at  $2\theta = 18.4$  corresponds to the repeat distance perpendicular to the tube, so the interlayer spacing ( $3.4\text{\AA}$ ) can be determined from the peak position, the number of concentric tubes from the FWHM of the peak and the distribution of spacings from the asymmetry. Here the FWHM corresponds to around 12 turns.

T5 - P106

## PARTICLE SIZE DISTRIBUTION FUNCTION OF SUPPORTED GOLD CATALYSTS BY X-RAY DIFFRACTION

C. Ducu<sup>1</sup>, V. Malinowski<sup>1</sup>, Mihaela Lazar<sup>2</sup>, N. Aldea<sup>2</sup>, I. Stefanescu<sup>1</sup>, I. Iosub<sup>1</sup>, P. Marginean<sup>2</sup>, B. Barz<sup>2</sup>

<sup>1</sup>University of Pitesti, Advanced Materials Department, Romania,  
[cd\\_Hlt76442318u\\_Hlt76442318cu@clubmed.ro](mailto:cd_Hlt76442318u_Hlt76442318cu@clubmed.ro)

<sup>2</sup>National Institute for Research and Development of Isotopic and Molecular Technologies, Romania

Pure gold was considered to be an uninteresting metal from the point of view of catalysis. Recently, was reported to be extremely active for some reactions if deposited as nanoparticles on different supports [1, 2]. In this paper the influence of the preparation method and support nature on

the structural properties of gold based catalysts are presented.

The preparation methods [1, 3, 4] are:

impregnation of the support with aqueous solution of  $\text{HAuCl}_4 \cdot 3\text{H}_2\text{O}$  in order to obtain 5 wt.% gold on supported catalysts;

*Size Distribution Function Au/SiO<sub>2</sub>*

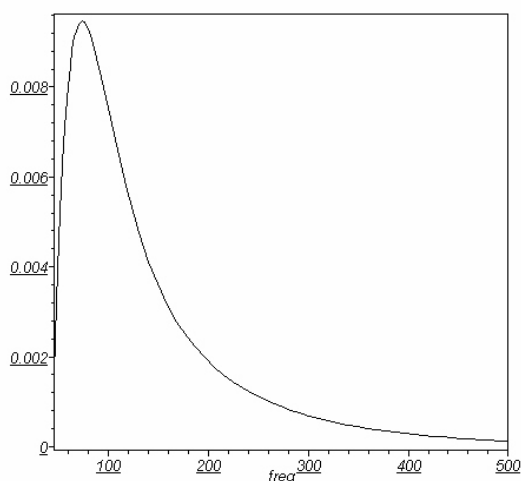


Figure 1

*Microstrain Distribution Function Au/SiO<sub>2</sub>*

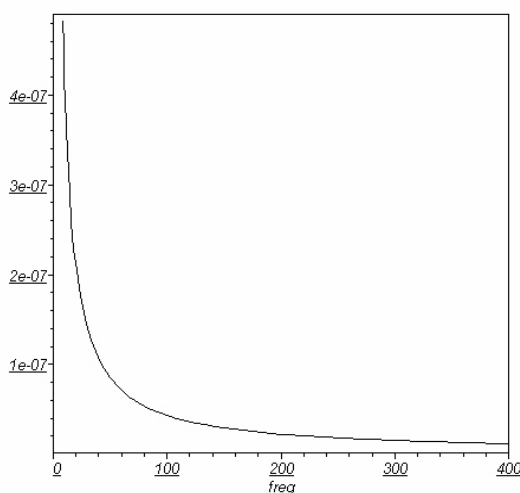


Figure 2

homogeneous deposition-precipitation using urea like precipitation agent. The suspension of support with  $\text{HAuCl}_4 \cdot 3\text{H}_2\text{O}$  was heated at ca.  $70^\circ\text{C}$ , under vigorous steering, in order to decompose the urea. The result was washed, dried in air at  $80^\circ\text{C}$  and then calcinated in airflow at ca.  $300^\circ\text{C}$ .

The following metal oxides, with high specific surface area were used as supports:  $\text{SiO}_2$ ,  $\text{Al}_2\text{O}_3$ ,  $\text{CeO}_2$ ,  $\text{Cr}_2\text{O}_3$ ,  $\text{Fe}_2\text{O}_3$ ,  $\text{ZrO}_2$  and  $\text{TiO}_2$ .

The supported Au catalysts were studied by X-ray diffraction in order to determine the average particle size, the mean squares of the microstrain, the probability of the faults, the particle size distribution and microstrain functions. The method is based on Fourier analysis of the experimental X-ray line profiles (XRLP) (111), (200), (220) and (311). The global structure is obtained with a fitting method based on the generalized Fermi function facilities [5,6]. The X-ray diffraction data of gold catalysts were collected at room temperature, using a horizontal powder goniometer in Bragg-Brentano (BB) geometry installed on DRON 2 setup connected with PC, containing a large spectra library. The incident Cu-K radiation was filtered with Ni foil,  $\lambda = 1.54178 \text{ \AA}$ . The typical experimental conditions were: 60 sec. for each step, initial angle  $2\theta = 10^\circ$ , step  $0.02^\circ$ , on 3500 points. The diffraction profiles were measured with a scintillation detector, single channel pulse-height discrimination and standard associated counting circuit.

Data processing is based on Warren-Averbach and Charlson approximations. The XRLP and their Fourier transform were approximated with the generalized Fermi

functions (GFF). Only the XRLP with a good S/N ratio were processed. In the case of multiple lines for one spectrum we were able to determine the crystallite morphology. It can be observed, for all the samples, a good correlation between the global structure parameters (i.e. small crystallite sizes imply large values for the microstrain and the faults probability). We have obtained crystallite sizes between 2.1 ( $\text{Au}/\text{Al}_2\text{O}_3$ ) and 28.5 nm ( $\text{Au}/\text{SiO}_2$ ) depending on the preparation method and the support nature. Figures 1 and 2 contain the size and the microstrain distribution functions for  $\text{Au}/\text{SiO}_2$  sample.

The aim of these studies is to understand the relation between the catalytic activity and the global microstructural model [4, 7].

1. M. Haruta, *Cattech* 6 (2002) 102;
2. G.C. Bond, D.T. Thompson, *Catal. Rev. - Sci. Eng.*, 41 (1999) 319;
3. A.C. Gluhoi, M.A.P. Dekkers, and B.E. Nieuwenhuys, *J. Catal.* 219 (2003) 197;
4. R. Grisel, K. Weststrate, Andreea Gluhoi and B. E. Nieuwenhuys, *Gold Bulletin* 2002 35/2 (2002) 45.
5. N. Aldea, Andreea Gluhoi, P. Marginean, C. Cosma, Xie Yaning, *Spectrochimica Acta A*, Part B 455 (2000) 997-1008;
6. N. Aldea, C. Tiusan and B. Barz, *Journal of Optoelectronics and Advanced Materials* Vol. 6 No. 1 (2004) 225;
7. N. Aldea, Andreea Gluhoi, P. Marginean, C. Cosma, Xie Yaning, Hu Tiandou, Whongua Wu and Baozhong Dong, *Spectrochimica Acta B* 57, 1453 (2002).

T5 - P107

## STRUCTURAL EVOLUTION AND SELECTIVITY OF THE DIOCTAHEDRAL 2:1 CLAY IN RELATION WITH THE CATION CONCENTRATION OF HEAVY METALS: XRD QUANTITATIVE ANALYSIS

W. Oueslati, H. Ben Rhaïem, M. S. Karmous & A. Ben Haj Amara

*Laboratoire de Physique des Matériaux, Faculté des Sciences de Bizerte Tunisia*

One of the environmental problems related to the modern world is the contamination of soil with heavy metals coming from household trash. The soil is a mixture of more or less coarse particles such as sand, gravel, clay.... Among this mixture, the clay fraction is characterised by the finest particle size ( $<2\mu\text{m}$ ) and represents the most active and efficient phase in the soil organisation and behaviour. The aim of this work is to characterise the structural evolution of a dioctahedral smectite (Wyoming montmorillonite) saturated with heavy metal cations. A quantitative analysis of XRD patterns is achieved using an indirect method based on the comparison of XRD experimental patterns to calculated ones. The study is achieved in two steps: 1) First the clay Cation Exchange Capacity (CEC) is saturated with one metallic cation  $\text{Ca}^{2+}$  or  $\text{Cu}^{2+}$  or  $\text{Ni}^{2+}$ . In fact  $\text{Ca}^{2+}$  is a dominant cation in soil clays, whereas  $\text{Cu}^{2+}$  and  $\text{Ni}^{2+}$  are two heavy metal cations occurring in household trash. The resulting complexes were respectively labelled Wy-Ca,

Wy-Cu and Wy-Ni. The quantitative analysis of the XRD patterns produced by these complexes shows that they are characterised by 12.4 Å, 15.43 Å and 15.06 Å respectively for Wy-Cu, Wy-Ca and Wy-Ni.

2) Secondly, the clay is placed in presence of a biionic solution: (Ca, Cu) or (Cu, Ni) in order to understand the selectivity of the clay for these cations. Figure I shows the evolution of the  $d_{001}$  spacing when increasing the solution concentration.

We notice that for low concentration the  $d_{001}$  spacing corresponds to the Wy-Cu complex whereas for high concentration, the  $d_{001}$  spacing can be attributed to the Wy-Ca or Wy-Ni. This means that at low concentration, the clay CEC is saturated with low hydration state cation (i.e.  $\text{Cu}^{2+}$ ) which is characterised by one water layer, for high concentration, the clay fixes the cation with high hydration state (i.e.  $\text{Ca}^{2+}$  or  $\text{Ni}^{2+}$ ) which are characterised by two water layers.

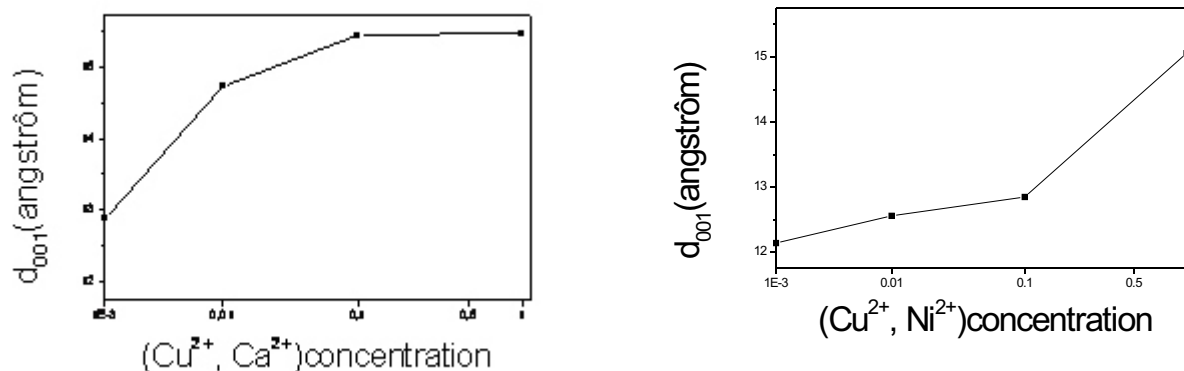


Figure 1. Evolution of the  $d_{001}$  versus the concentration of the different couples of cation

T5 - P108

## STRUCTURAL PROPERTIES OF SMECTITE SATURATED BY HEAVY METALS THERMALLY TREATED

Mohamed Salah Karmous, Hafsia Ben Rhaïem, Walid Oueslati & Abdesslem Ben Haj Amara

*Laboratoire de Physique des Matériaux, Faculté des Sciences de Bizerte, Tunisia*

The threat of environmental pollution from the release and dispersal of heavy metals accumulated in soil minerals led to extensive research focusing on the fixation of these heavy metals cations on smectites.

The main objective of this study is to investigate the intercalation and diffusion of heavy metals cations such as  $\text{Cu}^{2+}$  and  $\text{Ni}^{2+}$  into a Wyoming montmorillonite.

The Cation Exchange Capacity (CEC) of purified Wyoming montmorillonite, was saturated with  $\text{Cu}^{2+}$  or  $\text{Ni}^{2+}$  cations. The resulting complexes will be designed Wy-Cu and Wy-Ni.

The obtained samples were then heated at moderate temperature in order to trap definitively the different cations within the clay structure.

The quantitative analysis of XRD patterns using an indirect method allows us to characterise the structural evolution of these samples. The method permits to determine

the number and the position of the intercalated cations and water molecules in the interlamellar space. The comparison of experimental x-ray patterns to calculated ones use a structural model showed that: for the air-dry (1) the Wy-Cu complex is characterised by a basal spacing of 12.4 Å (2) The Ni-Wy air-dry sample is characterised by a basal spacing of 14.8 Å, these basal spacings correspond to one and two water layers between the silicate layers respectively for the Cu and Ni complexes.

After thermal treatment, the quantitative XRD analysis shows that: until 250°C, the basal spacing decreases until 10 Å. This decrease is attributed to the loss of interlamellar water. When increasing temperature up to 350°C, a proportion of  $\text{Cu}^{2+}$  and  $\text{Ni}^{2+}$  cations diffuses into the octahedral vacancies and this proportion increases when increasing the heating duration.

T5 - P109

## XRD STUDY OF THE STACKING MODE OF THE NACRITE/ALKALI HALIDES COMPLEXES

Naamen S., Ben Rhaïem H., Karmous M. S. & Ben Haj Amara A.

*Laboratoire de Physique des Matériaux, Faculté des Sciences de Bizerte, Tunisia*

The homogenous nacrite/CsCl, KCl and KBr complexes have been successfully prepared by immersing an homogeneous 8.4 Å hydrated nacrite in a CsCl, KCl or KBr saturated solutions. These three complexes have been studied using X-ray diffraction (XRD) and TG analysis. The qualitatively X-ray diffraction analysis was based on a comparison between the experimental and calculated patterns.

The XRD patterns showed basal spacing equal to 7.2 Å, 10.0 Å, 10.4 Å and 10.5 Å respectively for the non-treated nacrite, the nacrite/KCl, nacrite/KBr and nacrite/CsCl complexes. This result indicated the intercalation of the hydrated salts between the nacrite layers.

The qualitatively analysis of the diffraction patterns from these three complexes vary in resolution, intensity, and position: (1) the basal  $00l$  reflections indicate a large number of coherently scattering parallel layers; (2) the  $hkl$  reflections (with  $h$  and/or  $k \neq 0$ ) are broadened indicating a disorder structure in the  $(a, b)$  plane.

The determinations of the structural evolution were conducted in two steps: firstly, we studied the  $00l$  reflections using a direct method involving a monodimensional

electron density projection; secondly we studied the  $hkl$  reflections, with  $h$  and/or  $k \neq 0$ .

The direct method involving a monodimensional electron density projection, along the normal to the layers, is used to determine the number and the positions of the intercalated compounds. The better reliability factors obtained for these complexes nacrite/alkali halides are less than 5%.

For the complex nacrite/CsCl and nacrite/KBr, the cations are located near to the oxygen atom plane. The anions are situated above the hydroxyl groups and the H<sub>2</sub>O molecules in the middle of the interlamellar space.

For the complex nacrite/KCl, the cation, the anion and one H<sub>2</sub>O molecule are located respectively near the hydroxyl groups and another water molecule is situated under the oxygen atom plane for the second layer. These XRD results are consistent with those of TG analysis.

The study of the  $hkl$  reflections (with  $h$  and/or  $k \neq 0$ ), allowed the determination of the stacking mode and the position of the intercalated species in the  $(a, b)$  plane. The observed disorder of the XRD diagrams for these complexes are related to the existence of different sites occupied by the cations.

T5 - P110

## ATOMIC STRUCTURE OF Re-Tb AMORPHOUS ALLOYS

A. V. Bondarev, Yu. V. Barmin, I. L. Bataronov

*Voronezh State Technical University, 14 Moskovski prospect, 394026 Voronezh, Russia, e-mail: bondarev@vmail.ru*

The Re-Tb amorphous alloys with the terbium content of 18, 36, 53, 71 and 89 at.% were produced by three-electrode ion-plasma sputtering of a composite target. Composition of the alloys was determined by the electron-probe X-ray spectral microanalysis with the accuracy of 0.5 at.%.

The atomic structure of amorphous alloys was studied on the standard X-ray diffractometer in geometry of reflection using MoK $\alpha$  radiation ( $\lambda = 0.071$  nm) and a graphite monochromator in the diffracted beam. The scattering intensity  $I(\theta)$  was recorded by points within the range of scattering angles  $2\theta$  from 5° to 80°. The experimental curves  $I(\theta)$  were corrected for air background, polarization and absorption. Then the intensity was normalized into electronic units by the Krogh-Moe — Normann method. The structure factors (SF) were calculated taking into account intensity of incoherent radiation and corrections to anomalous dispersion of the atomic scattering factors [1].

The radial distribution function (RDF) can be obtained as the sine Fourier transformation of the SF. However, the

direct Fourier transformation is sensitive to such experimental errors in the structure factor as statistical dispersion and to the measurement on the finite interval. To reduce the effect caused by these errors, the following algorithm was used: the experimental SF is smoothed with a set of basic functions and then the Fourier transformation of the smoothed solution is performed. In this work we used the method based on separation of the SF into several intervals which corresponded to the different peaks on the SF. In each interval the experimental SF was approximated with a wave package (a set of basic functions) [2]. Application of this method considerably increases the accuracy of reconstruction of the RDF and provides stability to random experimental errors.

Using the reduced RDF  $G(r)$  and the total RDF, we calculated parameters of the topological short-range order. The radii of coordination spheres  $R_1$ ,  $R_2$ ,  $R_3$  and  $R_4$  were determined by positions of the corresponding maxima on the  $G(r)$  functions. Coordination number of the first sphere  $Z_1$  was calculated as the area under the first peak of the total



RDF. The mean-square deviations of the atomic positions in the first sphere ( $R_1$ ) was determined by the half-width of the first peak of the total RDF.

Radius of the first coordination sphere increases proportionally to concentration of the atoms with the greater diameter – terbium. The value of  $R_1$  grows from 0.278 nm for  $\text{Re}_{82}\text{Tb}_{18}$ , which is close to the atomic diameter of rhenium, to 0.355 nm for  $\text{Re}_{11}\text{Tb}_{89}$ , which coincides with the atomic diameter of terbium. The relative radii of the coordination spheres  $R_i/R_1$  do not depend on composition of the alloys within the all concentration interval. The average values  $R_2/R_1=1.67$ ,  $R_3/R_1=1.89$ ,  $R_4/R_1=2.54$  are close to the well-known values for the majority of metallic glasses.

The mean-square deviation of the atomic positions in the first sphere ( $R_1$ ) changes with the change of composition and it has the maximum value at  $x=36-71$  at.% Tb. The increase of the ( $R_1$ ) near the middle of the concentration interval is caused by high content of the atoms of the second component with the atomic diameter that considerably differs from the atomic diameter of the first component ( $d_{\text{Tb}}/d_{\text{Re}}=1.292$ ). Effect of increasing the dispersion of atomic positions with introducing atoms of the greater diameter into an amorphous matrix is also observed in the other binary amorphous systems: Re-Ta [3], Re-Nb and Re-Hf [4].

It was established that the basic parameters of topological short-range order in these AA do not depend on the composition. The relative radii of coordination spheres  $R_i/R_1$  remain unchanged. The coordination numbers of the first sphere  $Z_1$  also do not change as the composition varies.

It was proposed that local structural units in these amorphous alloys are coordination polyhedra of corresponding crystalline compounds. In the Re-Tb system such a com-

pound is close-packed tetrahedral crystalline structure (Laves phase).

Computer simulation of atomic structure of Re-Tb amorphous alloys was carried out using the molecular dynamics method. As an initial atomic configuration we chose random distribution of 7000 atoms inside the basic cube with periodical boundary conditions. For numerical solving the equations of motion the Verlet algorithm in the velocity form was used. Integration step was  $2 \cdot 10^{-15}$  s, relaxation was conducted during 5000 time steps. Simulation was conducted at constant temperature 300 K with correction of temperature on each time step by means of velocity scaling.

For description of interatomic interaction in the Re-Tb system we constructed the model potential represented as a polynomial of the fourth power [5]. Coefficients of the potential was calculated using the parameters for the crystalline analogues (atomization energy, bulk moduli, atomic volume).

The RDF calculated for the models are in good agreement with the experimental ones. For the models we calculated distributions of coordination numbers, distributions of bond angles, partial RDF and parameters of compositional short-range order.

- [1] C.N.J. Wagner, *J. Non-Cryst. Solids* 31 (1978) 1-40.
- [2] I.L. Bataronov, A.V. Bondarev, Yu.V. Barmin, *Bulletin of Russian Academy of Sciences* (2004) (in press).
- [3] Yu.V. Barmin, V.G. Samoiloov, I.L. Bataronov, S.A. Roshchupkin, *Ibid.* 61 (1997) 750-752.
- [4] Yu.V. Barmin, E.V. Lebedinskaya, I.L. Bataronov, A.V. Bondarev, *Mater. Sci. Forum* 321-324 (2000) 519-524.
- [5] I.L. Bataronov, A.V. Bondarev, Yu.V. Barmin, *Bulletin of Russian Academy of Sciences* 64 (2000) 1329-1332.

T5 - P111

## PREPARATION AND CHARACTERIZATION OF ISOMETRIC GOLD NANOPARTICLES WITH PRE-CALCULATED SIZE

M. Šlouf<sup>1</sup>, R. Kužel<sup>2</sup>, Z. Matěj<sup>2</sup>

<sup>1</sup>*Institute of Macromolecular Chemistry, Academy of Sciences of the Czech Republic, Heyrovského nam. 2, 162 06 Praha 6, Czech Republic*

<sup>2</sup>*Department of Electronic Structures, Faculty of Mathematics and Physics, Charles University, 121 16 Praha 2, Ke Karlovu 5, Czech Republic*

Nanoparticles of precious metals like gold, silver, platinum are intensively studied in last years. They found applications as surfaces in chemical analysis, as carriers of molecules, as markers in transmission electron microscopy (TEM) etc. Metal nanoparticles can compose more or less stable colloid solutions. Their size can be controlled by appropriately selected process of preparation. In this work, Au particles with different sizes were prepared and characterized in solution by UV/vis spectroscopy and in solid state by TEM and powder diffraction.

**Preparation of Au nanoparticles.** Preparation of colloidal Au nanoparticles was described as early as at the end of 19th century. We used a combination of the techniques al-

ready described. They were slightly modified so that we were able to obtain particles with arbitrary size. Our new technique is based on several-step reduction of  $\text{H}[\text{AuCl}_4]$  water solution by combination of  $\text{Na}[\text{BH}_4]$  and a  $\text{NH}_2\text{OH}$  solutions. The whole preparation procedure is as follows: (i) choice of average particle size  $d_{\text{theor}}$  (ii) calculation of solution concentrations, (iii) performing  $\text{H}[\text{AuCl}_4]$  reduction according to previous step and (iv) experimental determination of real average particle size  $d_{\text{exp}}$ . Usually it is found  $d_{\text{exp}} < d_{\text{theor}}$ , but the discrepancy is less than 20%. In this study we intended to prepare four different sets of particles, denoted as Au1, Au2, Au3 and Au4, with average sizes 4.5, 11.7, 35.0 and 105.8 nm, respectively.

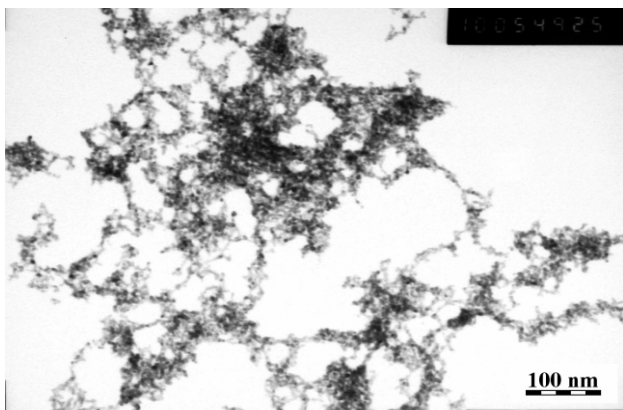


Fig 1. TEM microphotograph of colloid Au1

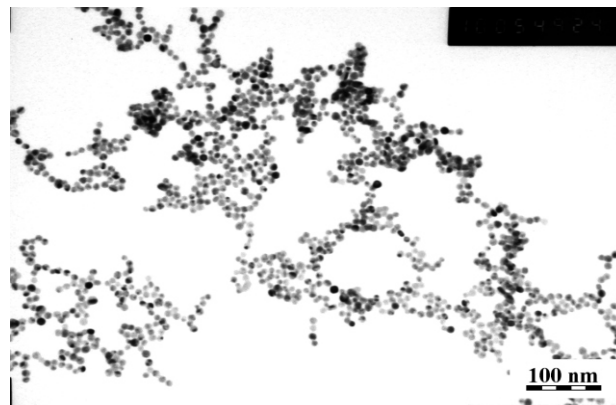


Fig 2. TEM microphotograph of colloid Au2

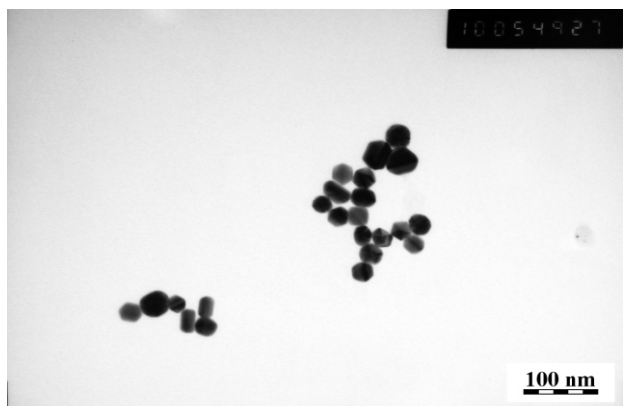


Fig 3. TEM microphotograph of colloid Au3

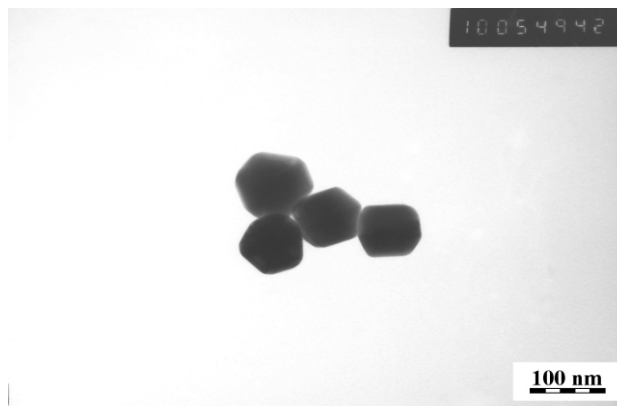


Fig 4. TEM microphotograph of colloid Au4

**UV/vis spectra.** Colloidal solutions of gold nanoparticles appear red in color. The exact hue of the solution depends, among other things, on the size of the particles and can be measured by means of UV/vis spectroscopy. UV/vis spectra of gold nanoparticles in water were measured in the range of wavelength  $\lambda = 300 - 900$  nm with step 2 nm.

**Transmission electron microscopy (TEM).** Approx. 2  $\mu$ l of Au colloidal solution was transferred to microscopic grid covered with carbon film and left to evaporate. Dry Au particles were examined in microscope JEM 200CX (Jeol, Japan). All TEM microphotographs were taken at acceleration voltage 100 kV, recorded on a photographic film and digitized with pc-controlled digital camera DXM1200 (Nikon, Japan). Image analysis of TEM micrographs was performed with program LUCIA (LIM, Czech Republic), Figs. 1-4.

**X-ray diffraction (XRD).** A film of colloidal Au particles were collected onto the surface of a microscopic glass and measured with a Philips X'Pert PRO diffractometer and a  $2\theta$  scan with the incidence angle  $\theta = 2^\circ$  in the parallel beam geometry. A pure glass substrate and a NIST LaB<sub>6</sub> standard were measured in the same instrumental arrangement and the same incidence angle to correct data for instrumental effects. Diffraction line broadening was analysed using Willimason-Hall (WH) plots and mainly the whole profile modelling (WPPM) approach with the program PM2000 [1-2] (Fig. 7). Surprising feature of studied samples is a strong anisotropy of line broadening and a sharp slope of the WH plot (Fig. 5). Anisotropy of line broadening can not be justified by the size broadening ef-

fect of any isometric shape of particules. The WPPM fit is improved if deformation and twin faults are included in the microstructure refinement (Figs. 6-7). A high probability  $P_{\text{twin}}$  of finding a twin fault appears, especially in samples with very small grains (Table. 1). It results in a larger size of grains indicated from x-ray analysis (Table. 1).

**Particle size & shape.** The agreement between the sizes theoretically calculated and those determined experimentally was quite good (Table 1.). The average sizes and shapes of the particles were determined by image analysis of TEM micrographs. The particles were quite isometric, approximately spherical in shape. The crystal planes were observable as well, especially for larger particles (Fig. 4).

**Comparison of results.** UV/vis spectra of the Au colloidal solution exhibit one local absorption maximum, denoted as  $\lambda_{\text{max}}$ . The maximum occurs due to surface plasmon absorption. According to theory,  $\lambda_{\text{max}}$  should shift slowly towards higher  $\lambda$  with increasing size of the particles. In our study the size of the particles  $d_{\text{exp}}$  was determined by TEM and corresponding shift of  $\lambda_{\text{max}}$  was clearly observed (Fig. 8). Moreover, it was found that  $\lambda_{\text{max}}$  is a linear function of  $d_{\text{exp}}$  in the whole range), which is in agreement with our previous studies.

X-ray results are in a good agreement with others for Au2-4. For Au1 the size is significantly higher. This is caused by the fact that both line broadening anisotropy and its increase with diffraction vector magnitude had to be accounted for which was possible by putting stacking faults and dislocations into the calculations. Finally, very good fits of diffraction patterns were obtained but physical inter-

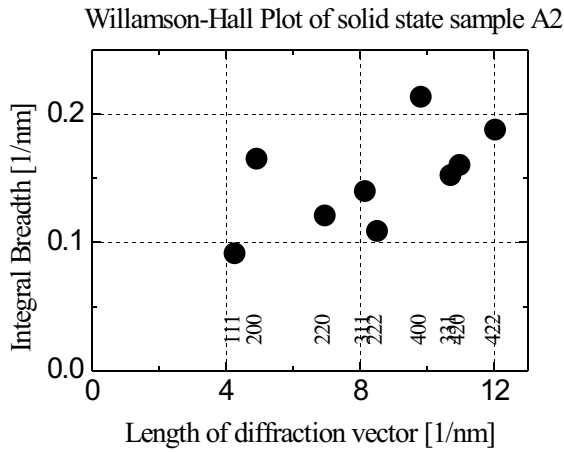


Fig 5. Williamson-Hall plot for A2.

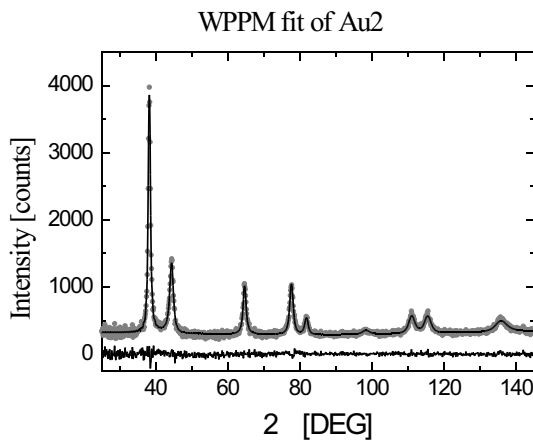


Fig 7. Whole profile modeling of diffraction pattern of Au2 using program PM2000 [1-2].

pretation of the parameters - twin faults and especially high dislocation densities of the order of  $10^{15} \text{ m}^{-2}$  (strains) should be further critically discussed and investigated.

**A new method for preparation of colloidal isometric Au nanoparticles** in solution was introduced. The size of the particles can be selected in advance within the range from 4.5 to 120 nm.

Size distribution of the particles exhibits gaussian shape. However, with increasing size of the particles the size distribution slightly broadens.

The Au nanoparticles with well-defined size can be employed in many fields. Our final goal is to use them as calibration particles for dynamic light scattering experiments.

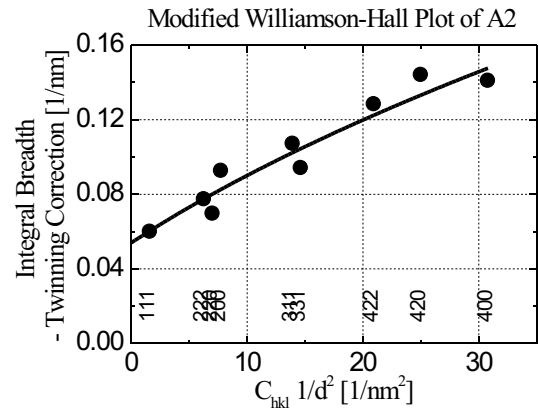


Fig 6. Modified Williamson-Hall plot for A2. Line broadening caused by twinning was subtracted from measured integral breadths.

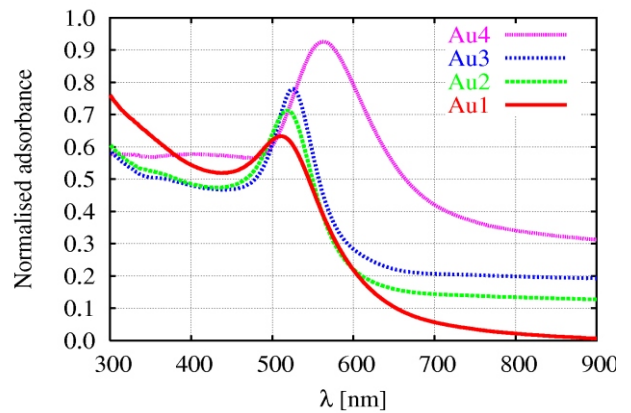


Fig 8. UV/vis spectra of colloidal solutions of Au1, Au2, Au3 and Au4.

**Table 1.** Agreement among theoretically calculated values of average diameter of the particles  $d_{\text{theor}}$ , experimentally determined average diameter  $d_{\text{exp}}$  and maximum of the absorption  $\lambda_{\text{max}}$ .

Koloid	$d_{\text{theor}}$ [nm]	$d_{\text{exp}}$ [nm]	$\lambda_{\text{abs}}$ [nm]	$d_{\text{diff}}$ [nm]	twin
Au1	4.5	4.3	512	11	0.08
Au2	11.1	8.8	519	17	0.07
Au3	33.4	28.3	525	29	0.04
Au4	101.5	84.5	563	119	0.005

*Acknowledgement*

This work was supported through grant GACR 106/04/1118 awarded by the Grant Agency of the Czech Republic.

[1] P.Scardi, M.Leoni, *Acta Cryst.* A58 (2002) 190-200.  
 [2] P.Scardi, M.Leoni, Y.H.Dong, *Eur. Phys. J. B* 18 (2000) 23-30.